

Chemical Science

Accepted Manuscript



This is an *Accepted Manuscript*, which has been through the Royal Society of Chemistry peer review process and has been accepted for publication.

Accepted Manuscripts are published online shortly after acceptance, before technical editing, formatting and proof reading. Using this free service, authors can make their results available to the community, in citable form, before we publish the edited article. We will replace this *Accepted Manuscript* with the edited and formatted *Advance Article* as soon as it is available.

You can find more information about *Accepted Manuscripts* in the [Information for Authors](#).

Please note that technical editing may introduce minor changes to the text and/or graphics, which may alter content. The journal's standard [Terms & Conditions](#) and the [Ethical guidelines](#) still apply. In no event shall the Royal Society of Chemistry be held responsible for any errors or omissions in this *Accepted Manuscript* or any consequences arising from the use of any information it contains.



www.rsc.org/chemicalscience

Cite this: DOI: 10.1039/c0xx00000x

www.rsc.org/chemicalscience

EDGE ARTICLE

Sequence-Responsive Unzipping DNA Cubes with Tunable Cellular Uptake Profiles

Katherine E. Bujold,^a Johans Fakhoury,^a Thomas G. W. Edwardson^a, Karina M. M. Carneiro^a, Joel Neves Briard,^a Antoine G. Godin,^b Lilian Amrein,^c Graham D. Hamblin,^a Lawrence C. Panasci,^{*c} Paul W. Wiseman^{*a,b} and Hanadi F. Sleiman^{*a}

Received (in XXX, XXX) Xth XXXXXXXXX 20XX, Accepted Xth XXXXXXXXX 20XX

DOI: 10.1039/b000000x

Here, we demonstrate a new approach for the design and assembly of a dynamic DNA cube with an addressable cellular uptake profile. This cube can be selectively unzipped from a 3D- to a flat two-dimensional structure in the presence of a specific nucleic acid sequence. Selective opening is demonstrated *in vitro* using a synthetic RNA marker unique to the LNCaP human prostate cancer cell line. A robust uptake in LNCaP cells, HeLa cells (human cervical cancer) and primary B-lymphocytes isolated from the blood of chronic lymphocytic leukemia (CLL) patients is observed using fluorescence-activated cell sorting (FACS), confocal microscopy and a new cluster analysis algorithm combined with image cross-correlation spectroscopy. The DNA cube was modified with hydrophobic and hydrophilic dendritic chains that were found to coat its exterior. The dynamic, unzipping properties of these modified cubes were retained, and assessment of cellular uptake shows that the hydrophobic chains help with the rapid uptake of the constructs while the hydrophilic chains become advantageous for long term internalization.

Introduction

DNA has emerged as a remarkable building material because of its programmability, biocompatibility, and its ready production and modification. These properties inspired the creation of the field of structural DNA nanotechnology^{1, 2} with the introduction of tile-based assembly^{3, 4} and DNA origami.⁵ Supramolecular DNA assembly^{6, 7} is a third strategy that focuses on the use of organic and inorganic synthetic molecules to guide structure formation and provide functionality to DNA nanostructures. Recent examples include the assembly of DNA-minimal prismatic structures and finely tuned nanotubes, and the creation of hydrophobic environments within these 3D-structures.⁷⁻¹¹

Small 3D DNA cages have recently attracted considerable interest since they can be readily taken up by cells,¹² they silence gene expression,¹³ they display higher serum stability^{14, 15} and have the potential to be precisely tailored in terms of size and shape for drug delivery applications. Many examples of DNA structures modified with biologically relevant moieties such as oligonucleotide drugs,^{13, 16-19} anticancer drugs,^{10, 20} aptamers,²⁰ biopolymers,²¹ or proteins²² have subsequently been presented. These demonstrate that small DNA cages can be used to target cells, encapsulate cargo and exhibit a cytotoxic effect in cancer cells. Hybrid structures which combine DNA with micelles or gold nanoparticles have also been shown to resist enzymatic degradation^{23, 24} and to result in gene knockdown.²⁵⁻²⁹ However, to our knowledge, precise control over the cellular delivery

profile of DNA nanostructures has yet to be demonstrated. In particular, synthetic modifications on the exterior of DNA cages can be used to tune and optimize their cellular delivery profiles as well as their nuclease resistance. However, these external modifications may impede the ability of DNA cages to undergo target recognition and dynamic behaviour.

In this article, we present a dynamic DNA cube design, which selectively opens up to form a two-dimensional structure upon recognition of a synthetic sequence of nucleic acids found in prostate cancer cells. We demonstrate the stability of this construct towards nucleases, its robust cellular uptake even in drug-resistant cell lines and its integrity upon cellular uptake. We modified this construct with hydrophobic and hydrophilic dendritic DNA chains to find that these coat the exterior of the structure and significantly alter its uptake profile, while maintaining its ability to unzip with the target sequence and stability in biological environments. Thus, this work provides a strong basis for the creation of DNA cages that can respond to nucleic acid sequences overexpressed in diseased cells, and that can be functionalized for finely tuned delivery profiles while retaining their dynamic character. The design can potentially be used to encapsulate and release or reveal sensitive cargo, (e.g. oligonucleotide drugs) and can be readily adapted to respond to a variety of targets.

Results and discussion

Cube design and self-assembly

The first DNA cube was designed as a cage that fully unfolds to a two-dimensional structure in the presence of a two-domain nucleic acid trigger, thereby revealing its inside. The chosen trigger was the mRNA product of the *tpc-hpr* fusion gene characteristic of a prostate cancer cell line (LNCaP). This gene was chosen because it produces unique DNA and mRNA sequences that contain specific parts of the *tpc* and *hpr* sequences around a fusion point (Figure 1d). Due to its uniqueness, this sequence was used for specific recognition and unwinding of the construct (Figure 2a-b). Since isolating this sequence from the cell in significant quantities proved challenging, we used shorter 21-base DNA and RNA versions of this marker which conserve the region of interest around the fusion point for cube opening experiments.

Structurally, this initial DNA structure is composed of six unmodified DNA strands that each form one of the faces of the cube, resulting in a fully double-stranded construct with 10 bases per side (full helix turn, ~ 3.4 nm) (Figure 1a). Two single-stranded overhangs were added which specifically recognize either the *tpc* or the *hpr* sequence immediately before the fusion point of the sequence (Figure 1c). However, the cube is designed to unfold by strand displacement only if the sequence after the fusion point corresponds to the other gene in the fusion. For example, if the overhang binds the *tpc* section of the sequence, the cube will only unfold if the *hpr* sequence follows after the fusion point. The cube will open after two binding events to produce a flat unzipped assembly by means of strategically placed nicks on the structure (Figure 2a-b, see movie in ESI). Due to its design, the cube is not expected to respond to the *tpc* or the *hpr* sequences alone.

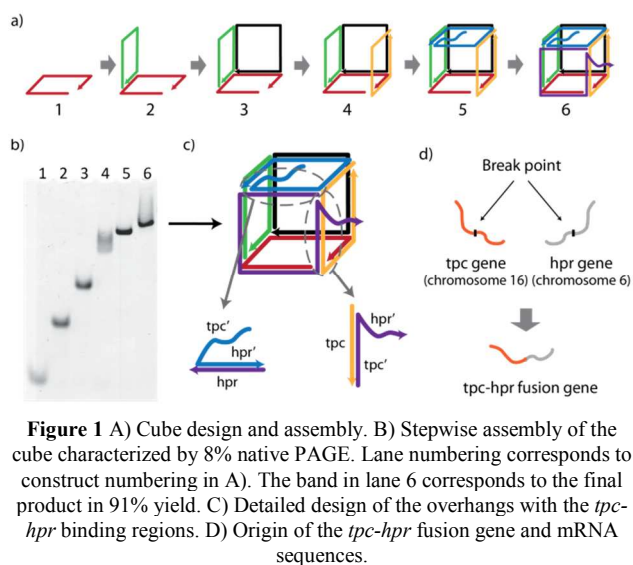


Figure 1 A) Cube design and assembly. B) Stepwise assembly of the cube characterized by 8% native PAGE. Lane numbering corresponds to construct numbering in A). The band in lane 6 corresponds to the final product in 91% yield. C) Detailed design of the overhangs with the *tpc-hpr* binding regions. D) Origin of the *tpc-hpr* fusion gene and mRNA sequences.

The successful assembly of this construct was verified by native polyacrylamide gel electrophoresis (PAGE) where each of the six strands involved in the formation of the cube was added sequentially (Figure 1b). The assembly was carried out by adding all six strands at a concentration of $0.27 \mu\text{M}$ in one pot in 1xTAMg buffer (see ESI) followed by thermal annealing from 95°C to 4°C in 5.5 hours. The major band in lane 6 was assigned to the cube which assembles with a yield of approximately 91%

(Figure S2). A small amount of side product was produced (Figure. 2c, lane 1) and was assigned as an octagonal prism composed of two cubes, or “double cube”, which in fact displays the same unfolding behaviour as the cube in the presence of the trigger (Figure S1). Moreover, its assembly yield can be reduced by using more dilute conditions.

Cube opening

Selective opening was examined next using PAGE (Figure 2c). Controls included the unzipping cube (lane 1) and an opened cube (lane 6) which does not have the proper sequence to close onto itself. The open cube shows a band of reduced mobility, compared to the more compact closed cube. When a short 21-base DNA segment with *tpc-hpr* fusion gene product sequence around the fusion point is added to the cube, a slower migrating band is obtained in lane 2, with the same mobility as that of the open cube. An identical synthetic RNA marker also opened the cube successfully *in vitro* and displayed equal unzipping potency (lane 3). Further testing was performed with DNA due to its enhanced stability towards degradation over RNA.

The specificity of the response was then tested by placing the cube in the presence of DNA strands of sequences *tpc* only (lane 4) and *hpr* only (lane 5). The cube mobility was not altered, consistent with the fact that these sequences did not trigger its opening. This confirms the specificity of cube unzipping that only responds to the *tpc-hpr* sequence expressed in prostate cancer cells, but not to *tpc* and *hpr* found in normal cells.

Cubes without overhangs were also tested to verify that the response is mediated by the single stranded regions of the construct (lanes 7, 8). In this case, the cube remained closed even in the presence of the *tpc-hpr* fusion marker, confirming that opening of the cube is strictly specific to this sequence when the recognition units are present. A cube with two different binding regions verified the stoichiometry of opening (lanes 9, 10).

Further assessment of the opening of the cube was done after modifying the structure with Cy3 (donor) and Cy5 (acceptor) dyes in a way such that when the cube is closed, the dyes are in close proximity and will undergo Förster resonance energy transfer (FRET) (Figure 2a and S5). However, when the cube is opened, these dyes will be spatially separated and the energy transfer between the dyes should be greatly reduced. This was done by on-column labelling one of the strands at its 5'-end with Cy5, and internally labelling a complementary strand with Cy3.

As expected, for all closed cube constructs, since the dyes were in close proximity, Cy3 excitation at 550 nm resulted in decreased Cy3 emission at 570 nm and increased Cy5 emission at 670 nm characteristic of FRET (Figure 2a-d). When the cube was unzipped, the donor emission was enhanced and the acceptor emission was reduced due to the increased distance between the fluorophores, consistent with successful opening. This was further quantified by looking at the efficiency of energy transfer between the dyes (E_{FRET}) for these constructs. Indeed, the closed cube had an efficiency of energy transfer of approximately 70%, while its opened counterparts only displayed 20% (Figure S6). The non-quantitative FRET efficiency in closed constructs was most likely due to the less than quantitative yield of labelling of the DNA strand with Cy5 at its 5'-end.

The same high E_{FRET} were also observed for the cube in presence of *tpc* only and *hpr* only, as well for the blunt-ended

Cite this: DOI: 10.1039/c0xx00000x

www.rsc.org/chemicalscience

EDGE ARTICLE

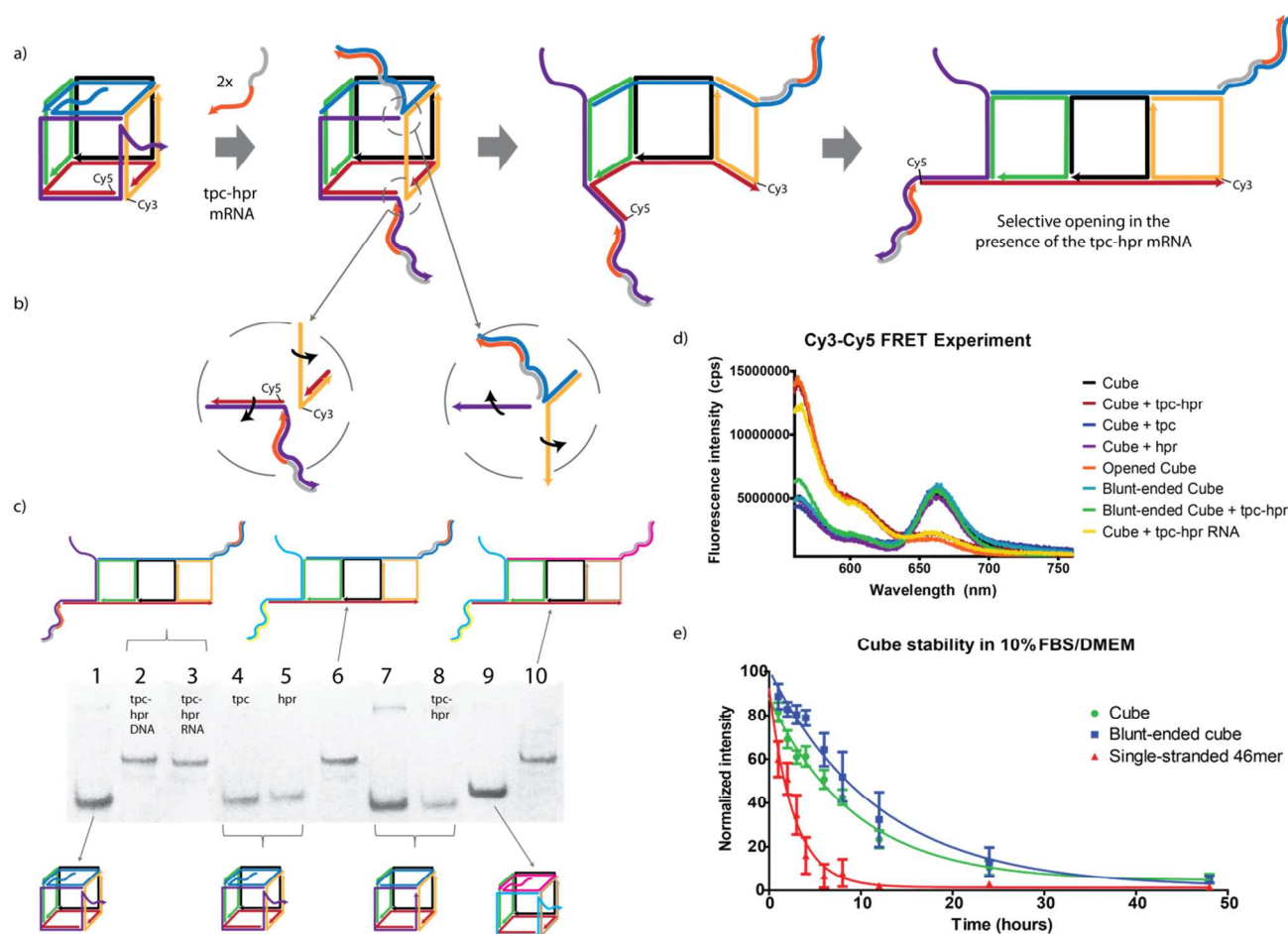


Figure 2 A) Cube opening schematic after the addition of two equivalents of the *tpc-hpr* fusion gene marker trigger. The trigger binds the overhangs and opens the cube by strand displacement and strategically placed nicks on the structure. This schematic also shows the dye placement. B) Detail of the junctions that allow the cube to open after strand displacement C) Cube opening characterized by 8% native PAGE. Lane 1 shows the cube as designed. The cube opens when *tpc-hpr* marker is present whether it is made of DNA (lane 2) or RNA (lane 3). *Tpc* alone (lane 4) and *hpr* alone (lane 5) markers fail to open the cube. An opened cube control (lane 6) and a blunt-ended cube (lane 7) which cannot open in presence of the marker (lane 8) were used to confirm the specificity of opening. A fully asymmetric cube (lane 9) was also prepared and opened (lane 10). D) Fluorescence emission spectra of different cube constructs after excitation at a wavelength of 550 nm. All closed constructs have decreased Cy3 emission at 570 nm and increased Cy5 emission at 670 nm due to FRET from the close proximity of both dyes. For the opened constructs, we observe enhanced donor emission and decreased acceptor emission since the dyes are now more separated in space. E) Stability in 10% FBS/DMEM of different constructs as measured by 8% native PAGE. One-phase decay regressions show that the cube has a half-life of 6.5 hours while the blunt-ended cube has a half-life of 8.2 hours.

cube with and without *tpc-hpr*, confirming that these constructs remained closed. Interestingly, the cube opened with the same efficiency using a DNA or RNA marker, confirming its relevance for cell-based assays (Figure 2d and S6). In principle, this cube should be adaptable for unzipping with a number of other DNA, RNA or miRNA sequences.

Cube stability

Preliminary evaluation of the cube robustness was carried out by measuring its melting temperature in phosphate buffer saline

(Figure S8). The measured melting temperature was 45°C, which suggests stabilization upon cube assembly (expected melting at 33.7°C for the 10-mer duplex arms) and is above the 37°C requirement for biological assays (Figure S8). We measured the stability of the cube in 10% FBS/DMEM media solutions using native PAGE according to the procedure developed by Conway *et al.*¹⁴ and showed that the cube has a half-life of 6.5 hours, (~3-fold increase over ssDNA) (Figure 2e and S9). The blunt-ended counterpart decays over 8.2 hours, suggesting the single stranded parts of the cube are susceptible towards enzyme degradation. In

Cite this: DOI: 10.1039/c0xx00000x

www.rsc.org/chemicalscience

EDGE ARTICLE

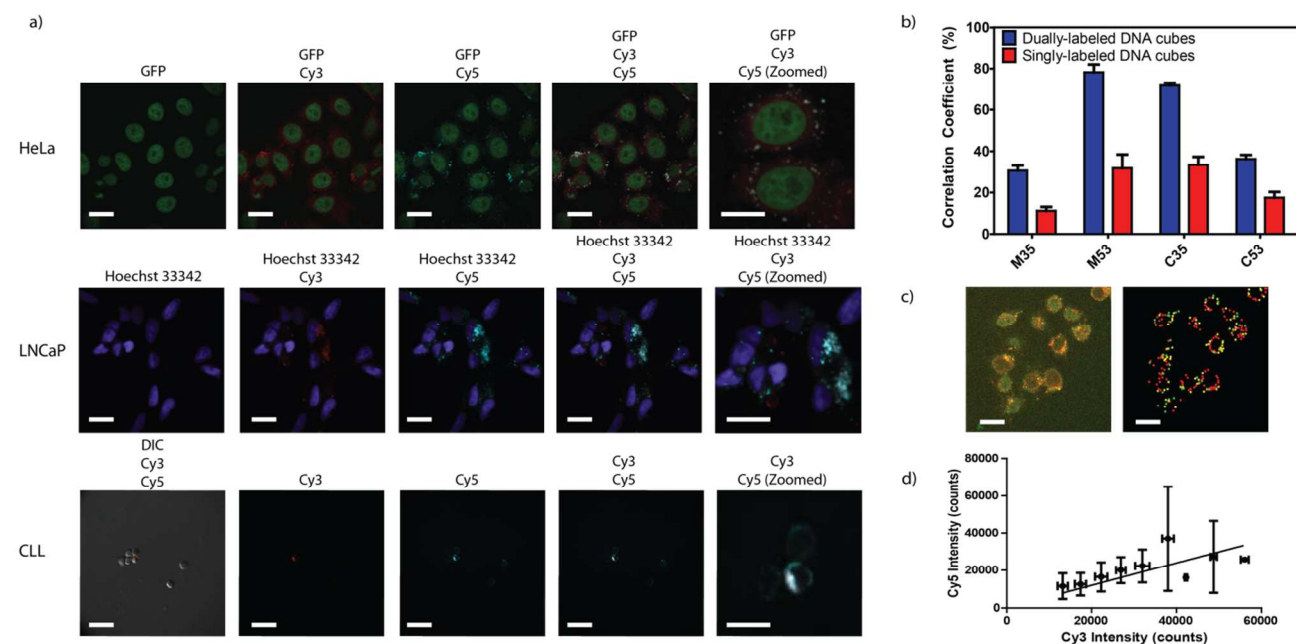


Figure 3 A) Cellular internalization of naked blunt-ended cubes labelled with Cy3 and Cy5 in three different cell types (scale bars: 20 μ m). B)

Colocalization correlation coefficients for dually-labelled cubes (blue) and a mixture of singly-labelled cubes (red) in HeLa cells. Single molecule colocalization coefficients (M35, M53) are obtained from image cross-correlation spectroscopy measurements. Spatial colocalization coefficients (C35, C53) are calculated from the spatial overlap of clusters in the images. For all coefficients, the dually-labelled cube (53 cells) is shown to exhibit higher colocalization than the mixture of singly-labelled cubes (32 cells). C) On the left, overlapping images of the initial confocal microscopy acquisitions with HeLa cells for both Cy3 (green) and Cy5 (red) channels. On the right, image processing results mapped to the image for the clusters detected by CF-ICCS (scale bars: 20 μ m). D) Bin plots of the fluorescence intensities of Cy3 versus Cy5 measured from images for spatially overlapping clusters for dually-labelled cubes in HeLa cells.

future cellular assays, these will therefore need to be replaced with synthetic nuclease resistant oligonucleotide analogues (such as locked nucleic acid or phosphorothioate DNA, however see below for stabilized forms of this cube). These assays confirmed the stability of the cube. Due to its significant resistance to enzymatic degradation, the blunt-ended construct was used for a preliminary evaluation of its cellular uptake.

Cellular uptake and structural integrity

Cube cellular uptake was first visualized by confocal microscopy, where cubes modified with Cy3 and Cy5 were incubated with HeLa cells for 6 hours prior to imaging. We used the blunt-ended construct for these assays due to its larger half-life which insured its structural integrity upon uptake and the ability to assess its uptake in the closed conformation. Both Cy3 and Cy5 channels indicated cellular uptake of the cube. An overlay of both channels showed consistent colocalization (Figure 3a). Similar results were obtained using the LNCaP human prostate cancer cell line (Figure 3a and S12). Remarkably, some uptake was also observed in drug resistant primary chronic lymphocytic leukemia (CLL) cells, further highlighting the potential of this construct for biological applications (Figure 3a and S13). The punctate structures observed suggest that the uptake likely occurs by endocytosis, a process often involved in the uptake of nucleic

acids.^{30, 31} Uptake of these naked DNA cubes in HeLa cells was also confirmed by fluorescence-activated cell sorting (FACS) (Figure S15).

In order to obtain more information on the structural integrity of the cube upon internalization in HeLa cells, we studied two populations: blunt-ended cubes dually labelled with Cy3 and Cy5, as well as a 1:1 mixture of singly labelled Cy3 and Cy5 blunt-ended cubes. Typical methods to track internalization involve measuring the spatial colocalization of these two fluorophores (see above). We thus first defined a 'cluster', as an arrangement of pixels with an intensity greater than a set threshold (for each fluorophore), and a radius above 0.3 μ m. We developed a cluster finding algorithm (named CF) that identifies these clusters for both fluorophores within images obtained from confocal microscopy (Figure 3c). We defined a cluster as being colocalized with another when its centroid was found to be localized in the mask of the other (Figure 3c and S17). For all colocalized clusters, the intensities of Cy5 vs. Cy3 were plotted and a linear trend was revealed (Figure 3d and S18). Interestingly, the slopes for both dually labelled cubes, and 1:1 monolabeled cube mixtures were equal, within statistical error (Figure 3d and S18, Table S9). This suggests compartmentalization of these labelled cubes upon cellular

Cite this: DOI: 10.1039/c0xx00000x

www.rsc.org/chemicalscience

EDGE ARTICLE

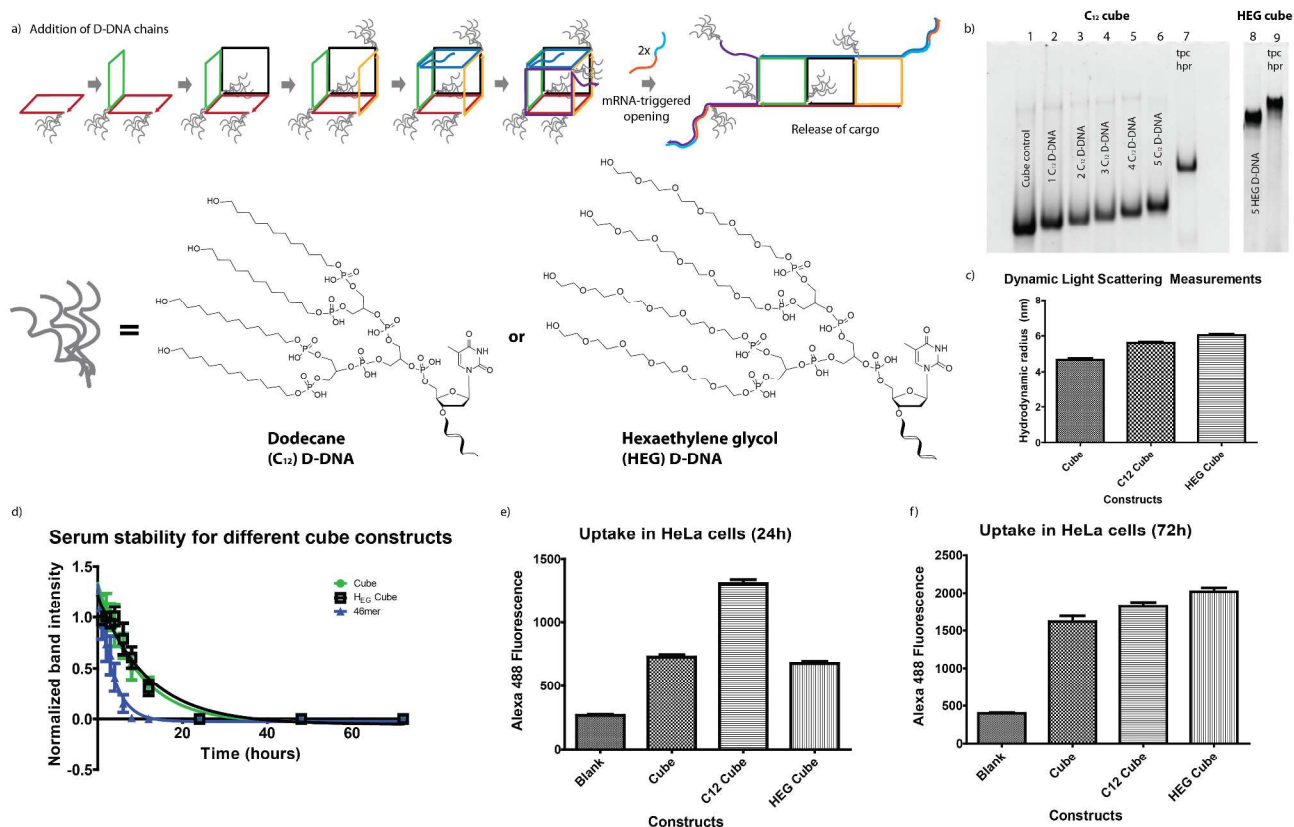


Figure 4 A) Cube modification with C₁₂ and HEG D-DNA schematic. B) On the right, C₁₂ cube stepwise assembly and opening. Lane 1 is the unmodified cube control, lanes 2-6 represent the subsequent addition of 1 up to 5 C₁₂ D-DNA chains on the structure. Lane 7 represents the fully D-DNA modified cube in presence of the *tpc-hpr* marker and its unhindered opening. Lane 8 is the fully modified HEG D-DNA cube and lane 9 shows the opened version of this construct when put in the presence of the *tpc-hpr* marker. C) Hydrodynamic radii of these cube constructs, the cube appears to be the smallest structure followed by the C₁₂ cube and the HEG cube. D) Serum stability of the different cube constructs. The C₁₂ cube has the longest half-life (8.3 hours) followed by the HEG cube (7.8 hours). E) FACS uptake of the three cubes after 24 hours. The C₁₂ cube presents the highest uptake compared to the other two constructs. F) FACS uptake of the three cubes after 72 hours. The HEG cube seems to be favoured over long time periods.

internalization, and a likely endosomal uptake mechanism, consistent with previous observations.³² Spatial colocalization coefficients C35 and C53 were calculated using these clusters (e.g. C35=number of Cy3 clusters colocalized with Cy5 clusters/total number of Cy3 clusters, Figure 3b). We noted that C35 and C53 are different from each other, most likely due to factors such as different bleaching properties and signal to noise ratios of fluorophores, as well as FRET. More importantly, the above spatial colocalization coefficients are limited by the intrinsic resolution of fluorescence microscopy (200 nm), considering that the DNA cube is expected to have a size of approximately 7 nm. To address this, we applied image cross-correlation spectroscopy (ICCS) to the identified clusters.³³ From the relative fluctuations in fluorescence intensities of the Cy3 and Cy5 dyes, correlation coefficients termed M35 and M53 were calculated, which provide a more representative representation of the cellular colocalization of these dyes at the single molecule level. From these, we observed colocalization of the two dyes,

with consistently higher colocalization coefficients for the dually labeled cube than the mixture of singly labeled cubes (Figure 3b). These results suggest that the DNA cubes maintain their integrity upon cellular internalization. To our knowledge, this is the first application of ICCS in tracking and quantifying DNA nanostructures in cellular environments.

Cube modification with dendritic chains

In order to modulate the uptake profile of the cube, the latter was modified with hydrophobic and hydrophilic dendritic DNA chains (D-DNA) (Figure 4a). The hydrophobic chains, C₁₂ D-DNA, were synthesized via phosphoramidite chemistry using automated methods.¹⁰ They consist of four hydroxyl-terminated dodecane (C₁₂) chains connected to two subsequent branching units on the 5'-end of the DNA chains involved. The hydrophilic chains, termed HEG D-DNA were synthesized using the same procedure as for the C₁₂ D-DNA, replacing the dodecane chains with hexaethylene glycol (HEG).³⁴

The D-DNA chains were added on five out of the six constituent strands of the cube. The sixth strand was left unmodified since adding the D-DNA would interfere with the single-stranded overhang on the 5'-end which is required for opening. The modified strands were characterized using denaturing PAGE and LC-MS to confirm both purity and the presence of the expected dendritic chains (Table S2).

The assembly of the cube with **C₁₂ D-DNA**, termed **C₁₂ cube**, was carried next using native PAGE adding one up to five chains on the structure (Figure 4b, lanes 2-6). Lower mobility bands were obtained every time a D-DNA chain was added, suggesting larger structures were formed. The full construct with five D-DNA chains was formed in quantitative yield with no observable octagonal prism side product (lane 6). Cubes that are externally coated with hydrophilic or hydrophobic chains may not be accessible for target triggered unzipping. Interestingly, opening was verified using native PAGE and was unhindered by the presence of the D-DNA chains on the cube as can be seen from the lower mobility bands obtained when adding an excess (2x) of the DNA marker (lane 7).

The dendritic alkyl chains in the **C₁₂ cube** can reside on the exterior of the cage, or these hydrophobic chains may be able to direct themselves into the inside of this cage. Our evidence points to these chains residing on the exterior. If the D-DNA chains were on the interior, we would expect similar mobility by gel, a size comparable to that of unmodified cube by DLS, and the ability to encapsulate dyes.¹⁰ If on the other hand, they are on the outside, we would expect lower mobility by PAGE, larger size, and inability to encapsulate. By gel electrophoresis, we obtained lower mobility bands as more **C₁₂ D-DNA** chains were added (Figure 4b, S3 and S4) suggesting that larger structures were formed. These results were confirmed by dynamic light scattering (DLS) where the **C₁₂ cube** presented a significantly larger hydrodynamic radius (5.6 ± 0.2 nm) than the unmodified cube (4.7 ± 0.3 nm) (Figure 4c, S11, Table S7). Attempts at encapsulating fluorescent dyes such as Nile Red and 1,6-diphenyl-1,3,5-hexatriene (DPH) which are used to detect a sizable hydrophobic environment were unsuccessful in the case of the **C₁₂ cube**, further suggesting that the **C₁₂ D-DNA** chains did not meet in the cavity of the cube as was observed by Edwardson *et al.*,¹⁰ but rather are coating the exterior of the structure (Figure S7).

Similar results were obtained for the **HEG D-DNA** modified cube, or **HEG cube**. Lower mobility bands were consistently obtained for the fully assembled structure with five **HEG D-DNA** chains by PAGE (Figure 4b, lane 8, S3 and S4) and the newly formed cage could open unhindered when an excess of DNA marker was added (lane 9). Yields were also found to be quantitative with no side product observed. Dynamic light scattering results showed that the **HEG** modified cages displayed the largest hydrodynamic radius of the set (6.0 ± 0.2 nm), thus supporting the positioning of the dendritic chains on the outside of the structure (Figure 4c, S11, Table S7). Moreover, the **HEG D-DNA** chains are more hydrophilic than the **C₁₂** chains and also likely extend outwards, thus explaining the larger hydrodynamic radius observed for the **HEG** cube when compared to the **C₁₂** construct whose dendritic chains present hydrophobic character and would be expected to collapse on each other (Figure 4a).

Differential cellular uptake of D-DNA modified cubes

Before proceeding to evaluate the uptake of these constructs in cells, we assessed their stability in 10% FBS/DMEM media solutions under native conditions using the procedure described above. We measured a half-life of 8.1 hours for the **HEG** cube containing the overhangs for unzipping, which was the longest of the set (Figure 4d). When compared to the unmodified cube (half-life of 6.5 hours), it seems that the **HEG D-DNA** chains contributed to enhance the stability of the cube in the cell-like environments, bringing it to the same level than the blunt-ended cube while keeping the single-stranded overhangs on the structure. On the other hand, the half-life of the **C₁₂ cube** could not be measured since it appears to bind to serum proteins found in FBS, as can be seen from the non-penetrating material in the gels (Figure S10). As a result, the **C₁₂ cube** levels could not be accurately quantified. This is probably due to the lipophilic chains which coat the cage and can bind albumin, a protein found in serum which acts as a carrier of molecules with low water solubility. Nevertheless, this binding to albumin may prove useful for delivery, and albumin-based drug formulations are currently used in the clinic.^{35,36} In the current system, serum proteins seem to be protecting the DNA structures from nucleases as can be seen from the leftover material in the lane after 72 hours (Figure S10).^{35,36}

In order to evaluate the impact of the **C₁₂** and **HEG D-DNA** external modifications on cube cellular uptake, we labelled these structures with Alexa-488, a dye similar to fluorescein which should have a limited impact on uptake since it is hydrophilic and negatively charged. The cellular uptake in HeLa cells of all three constructs was assessed using FACS. Results after 24-hour incubation show that the uptake of the **C₁₂ cube** is almost doubled when compared to the unmodified cube and the **HEG** cube (Figure 4e). The uptake was also verified by confocal microscopy (Figure S14). At the 48-hour time point, the **C₁₂ cube** was still dominant with the unmodified and the **HEG** cubes at equal levels (Figure S16). However, after 72 hours, the **HEG** construct was slightly favoured compared to the **C₁₂ cube** (Figure 4f). Both D-DNA modified constructs were still found in significantly higher amounts when compared to the unmodified cube, suggesting these constructs could be used in applications where the delivery profile is important; i.e. rapid distribution in the case of the **C₁₂ cage** or slow and continuous uptake like with the **HEG** construct.

Conclusions

In conclusion, we designed, assembled and characterized the first dynamic DNA cube that selectively unzips into a flat open structure, in the presence of a synthetic nucleic acid marker. This cube displays robust uptake in its naked form into three mammalian cells lines, including drug resistant primary B-CLL lymphocytes. We have applied image cross-correlation spectroscopy to confirm the colocalization of two dyes on dually labelled cubes within the cellular environment. Functionalizing the cube with hydrophobic or hydrophilic dendritic DNA chains significantly altered its uptake profile, thus allowing its cellular uptake to be tuned. The hydrophobic chains on the cube exterior seem to favour rapid and increased uptake while the hydrophilic chains provide a slow and continuous uptake profile. The

hydrophilic dendritic chains were also found to improve their nuclease resistance. Interestingly, these modified cubes are also capable of opening in response to a specific DNA sequence. This indicates that DNA structures can remain dynamic and molecule-responsive even when coated with lipid or PEG-like chains. This platform thus represents a first step in temporal as well as molecular control of DNA cage delivery. As such, this class of DNA structures has significant potential as cellular reporters, drug delivery tools and for the selective targeting of a specific biological pathway in a cellular environment. Future work is aimed at encapsulating and performing selective delivery of sensitive cargo (e.g., small interfering RNA) into disease environments.

Acknowledgements

We thank NSERC, FQRNT, CSACS and Prostate Cancer Canada through the Movember Discovery Grants for funding and Christian Young at the Lady Davis Institute Cell Imaging Facilities.

Notes and references

^a Department of Chemistry and Centre for Self-Assembled Chemical Structures (CSACS), McGill University, 801 Sherbrooke St. W., Montréal, Canada, H3A 0B8. Fax: +1-514-398-3797; Tel: +1-514-398-2633; E-mail: hanadi.sleiman@mcgill.ca

^b Department of Physics, McGill University, 3600 University St., Montréal, Canada, H3A 2T8.

^c Department of Oncology, Jewish General Hospital, 3755 Côte Sainte-Catherine Rd., Montréal, Canada, H3T 1E2.

† Electronic Supplementary Information (ESI) available. See DOI: 10.1039/b000000x/

- N. C. Seeman, *Nature*, 2003, **421**, 427-431.
- N. C. Seeman, *Molecular biotechnology*, 2007, **37**, 246-257.
- C. Lin, Y. Liu, S. Rinker and H. Yan, *ChemPhysChem*, 2006, **7**, 1641-1647.
- B. Wei, M. Dai and P. Yin, *Nature*, 2012, **485**, 623-626.
- P. W. K. Rothmund, *Nature*, 2006, **440**, 297-302.
- F. A. Aldaye, A. L. Palmer and H. F. Sleiman, *Science*, 2008, **321**, 1795-1799.
- C. K. McLaughlin, G. D. Hamblin and H. F. Sleiman, *Chemical Society Reviews*, 2011, **40**, 5647-5656.
- P. K. Lo, P. Karam, F. A. Aldaye, C. K. McLaughlin, G. D. Hamblin, G. Cosa and H. F. Sleiman, *Nat Chem*, 2010, **2**, 319-328.
- C. K. McLaughlin, G. D. Hamblin, K. D. Hänni, J. W. Conway, M. K. Nayak, K. M. M. Carneiro, H. S. Bazzi and H. F. Sleiman, *Journal of the American Chemical Society*, 2012, **134**, 4280-4286.
- T. G. W. Edwardson, K. M. M. Carneiro, C. K. McLaughlin, C. J. Serpell and H. F. Sleiman, *Nat Chem*, 2013, **5**, 868-875.
- G. D. Hamblin, A. A. Hariri, K. M. M. Carneiro, K. L. Lau, G. Cosa and H. F. Sleiman, *ACS Nano*, 2013, **7**, 3022-3028.
- A. S. Walsh, H. Yin, C. M. Erben, M. J. A. Wood and A. J. Turberfield, *ACS Nano*, 2011, **5**, 5427-5432.
- J. J. Fakhoury, C. K. McLaughlin, T. W. Edwardson, J. W. Conway and H. F. Sleiman, *Biomacromolecules*, 2013, **15**, 276-282.
- J. W. Conway, C. K. McLaughlin, K. J. Castor and H. Sleiman, *Chemical Communications*, 2013, **49**, 1172-1174.
- J.-W. Keum and H. Bermudez, *Chemical Communications*, 2009, 7036-7038.
- H. Lee, A. K. R. Lytton-Jean, Y. Chen, K. T. Love, A. I. Park, E. D. Karagiannis, A. Sehgal, W. Querbes, C. S. Zurenko, M. Jayaraman, C. G. Peng, K. Charisse, A. Borodovsky, M. Manoharan, J. S. Donahoe, J. Truelove, M. Nahrendorf, R. Langer and D. G. Anderson, *Nat Nano*, 2012, **7**, 389-393.
- J. Li, H. Pei, B. Zhu, L. Liang, M. Wei, Y. He, N. Chen, D. Li, Q. Huang and C. Fan, *ACS Nano*, 2011, **5**, 8783-8789.
- J.-W. Keum, J.-H. Ahn and H. Bermudez, *Small*, 2011, **7**, 3529-3535.
- X. Liu, Y. Xu, T. Yu, C. Clifford, Y. Liu, H. Yan and Y. Chang, *Nano Letters*, 2012, **12**, 4254-4259.
- M. Chang, C.-S. Yang and D.-M. Huang, *ACS Nano*, 2011, **5**, 6156-6163.
- D. Bhatia, S. Surana, S. Chakraborty, S. P. Koushika and Y. Krishnan, *Nat Commun*, 2011, **2**, 339.
- S. Juul, F. Iacovelli, M. Falconi, S. L. Kragh, B. Christensen, R. Fröhlich, O. Franch, E. L. Kristoffersen, M. Stougaard, K. W. Leong, Y.-P. Ho, E. S. Sørensen, V. Birkedal, A. Desideri and B. R. Knudsen, *ACS Nano*, 2013, **7**, 9724-9734.
- D. S. Seferos, A. E. Prigodich, D. A. Giljohann, P. C. Patel and C. A. Mirkin, *Nano Letters*, 2008, **9**, 308-311.
- A. M. Rush, M. P. Thompson, E. T. Tatro and N. C. Gianneschi, *ACS Nano*, 2013, **7**, 1379-1387.
- F. E. Alemdaroglu, N. C. Alemdaroglu, P. Langguth and A. Herrmann, *Macromolecular Rapid Communications*, 2008, **29**, 326-329.
- T. Chen, C. S. Wu, E. Jimenez, Z. Zhu, J. G. Dajac, M. You, D. Han, X. Zhang and W. Tan, *Angewandte Chemie International Edition*, 2013, **52**, 2012-2016.
- N. L. Rosi, D. A. Giljohann, C. S. Thaxton, A. K. R. Lytton-Jean, M. S. Han and C. A. Mirkin, *Science*, 2006, **312**, 1027-1030.
- D. A. Giljohann, D. S. Seferos, A. E. Prigodich, P. C. Patel and C. A. Mirkin, *Journal of the American Chemical Society*, 2009, **131**, 2072-2073.
- A. E. Prigodich, D. S. Seferos, M. D. Massich, D. A. Giljohann, B. C. Lane and C. A. Mirkin, *ACS Nano*, 2009, **3**, 2147-2152.
- S. Kawakami, Y. Higuchi and M. Hashida, *Journal of Pharmaceutical Sciences*, 2008, **97**, 726-745.
- D. Luo and W. M. Saltzman, *Nat Biotech*, 2000, **18**, 33-37.
- M. Elsabahy, A. Nazarali and M. Foldvari, *Current Drug Delivery*, 2011, **8**, 235.
- J. W. Comeau, S. Costantino and P. W. Wiseman, *Biophysical journal*, 2006, **91**, 4611-4622.
- K. M. M. Carneiro, F. A. Aldaye and H. F. Sleiman, *Journal of the American Chemical Society*, 2009, **132**, 679-685.
- D. D. Von Hoff, T. Ervin, F. P. Arena, E. G. Chiorean, J. Infante, M. Moore, T. Seay, S. A. Tjulandin, W. W. Ma, M. N. Saleh, M. Harris, M. Reni, S. Dowden, D. Laheru, N. Bahary, R. K. Ramanathan, J. Taberner, M. Hidalgo, D. Goldstein, E. Van Cutsem, X. Wei, J. Iglesias and M. F. Renschler, *New England Journal of Medicine*, 2013, **369**, 1691-1703.
- D. D. Von Hoff, R. K. Ramanathan, M. J. Borad, D. A. Laheru, L. S. Smith, T. E. Wood, R. L. Korn, N. Desai, V. Trieu, J. L. Iglesias, H. Zhang, P. Soon-Shiong, T. Shi, N. V.

Rajeshkumar, A. Maitra and M. Hidalgo, *Journal of Clinical Oncology*, 2011, **29**, 4548-4554.